Design, implementation, and characterization of an optical power supply spot-array generator for a four-stage free-space optical backplane

R. Iyer, Y. S. Liu, G. C. Boisset, D. J. Goodwill, M. H. Ayliffe, B. Robertson, W. M. Robertson, D. Kabal, F. Lacroix, and D. V. Plant

The design and implementation of a robust, scalable, and modular optical power supply spot-array generator for a modulator-based free-space optical backplane demonstrator is presented. Four arrays of 8×4 spots with 6.47-μm radii (at $1/e^2$ points) pitched at 125 μm in the vertical direction and 250 μm in the horizontal were required to provide the light for the optical interconnect. Tight system tolerances demanded careful optical design, robust optomechanics, and effective alignment techniques. Issues such as spot-array generation, polarization, power efficiency, and power uniformity are discussed. Characterization results are presented. © 1997 Optical Society of America

Key words: Optical power supply, spot-array generator, modulators, self-electro-optic devices, optomechanics, optical design, alignment, module, characterization.

1. Introduction

Current high-performance switching and computing systems rely mainly on electrical interconnection networks to transport information from chip to chip and board to board. However, electrical interconnects are limited by bandwidth, connectivity, power-consumption, and latency constraints. Because the aggregate bandwidth of the integrated circuits inside these systems continues to increase, so must the capabilities of the interconnection network.[1,2] The intrinsic limitations of electrical interconnection networks has led system designers to consider short-distance optical interconnects as a means of increasing their performance.[3–13] The optoelectronic technologies being considered include two-dimensional arrays of both surface-emitting and modulator-based devices integrated with arrays of electronic processing elements, called smart-pixel arrays (SPA's). A class of SPA's well suited for optical backplane interconnection applications uses the hybrid-SEED (self-electro-optic device) technology. This technology combines quantum-confined Stark effect modulators and p-i-n photodiodes (GaAs) with underlying silicon processing electronics.[14,15]

Because this type of smart pixel operates in the transmit mode by modulating an incident beam, systems that use this technology require optical power supply (OPS) beams to illuminate these reflective devices. The current state of affairs shows that there is a generation gap between the evolution of the sophisticated optoelectronics and the optics and optical packaging necessary to drive them. Recently, we designed and are in the process of completing a four-stage optical backplane demonstration system that uses hybrid-SEED SPA's[7] to study this problem. In this paper we describe the design, implementation, and characterization of an OPS spot-array-generator system built to bridge this generation gap. A full description of the optical design for the system was reported in Ref. 16, and the optomechanical design was presented in Ref. 17.

We begin in this paper by describing in Section 2 the requirements for the OPS. In Section 3 we explain the light source and distribution. In Section 4

R. Iyer, Y. S. Liu, G. C. Boisset, M. H. Ayliffe, B. Robertson, D. Kabal, F. Lacroix, and D. V. Plant are with the Department of Electrical Engineering, McGill University, Montreal H3A 2A7, Canada. When this study was performed, D. J. Goodwill was with the Department of Electrical and Computer Engineering, University of Colorado, Boulder, Colorado 80309; he is now with the Department of Interconnect Technology, Nortel, P.O. Box 3511, Station C, Ottawa, Ontario K1Y 4H7, Canada. W. M. Robertson is with the Department of Physics, Middle Tennessee State University, Murfeesboro, Tennessee 37132.

Received 4 March 1997; revised manuscript received 15 July 1997.

0003-6935/97/09230-13$10.00/0

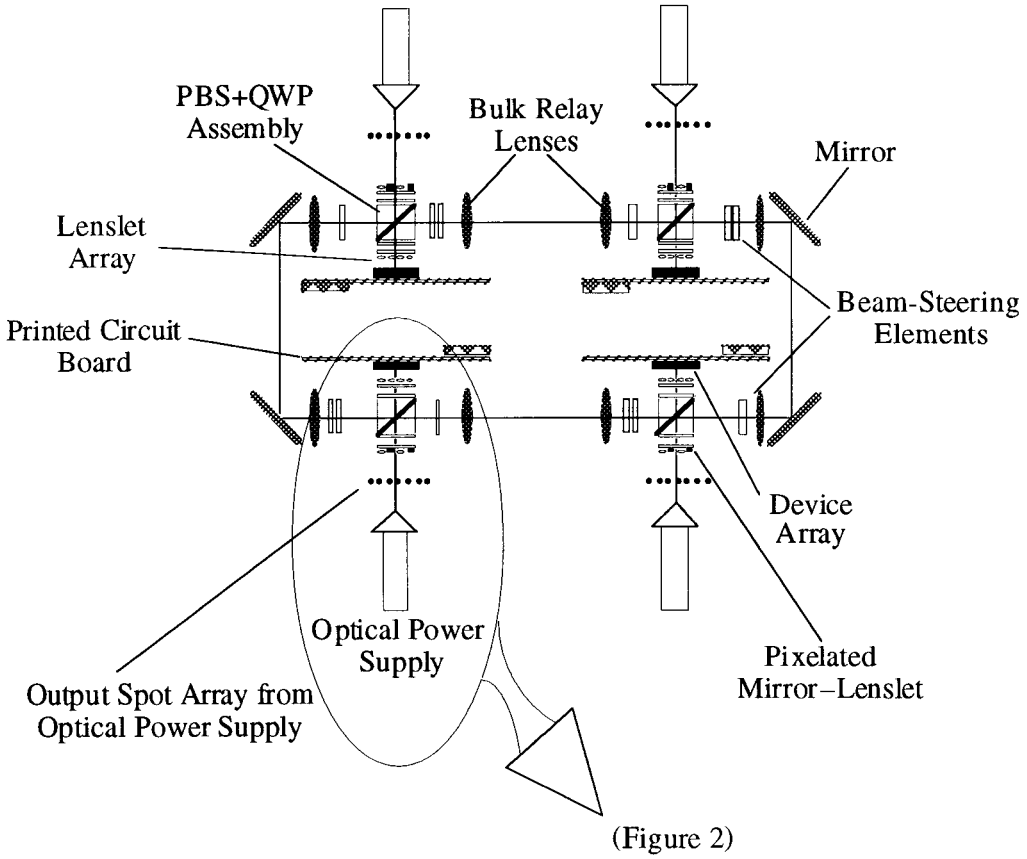

Fig. 1. Schematic of the unfolded OPS spot-array generator for a four-stage free-space optical backplane.

we describe in detail the optical design, and in Section 5 we present the optomechanics. In Sections 6 and 7 we present the assembly and alignment methodology and the characterization results, respectively.

2. Optical Power Supply Requirements

A. System Overview

The system was built in a three-dimensional layout interconnecting four hybrid-SEED SPA's in a unidirectional ring.[7] The chips were obtained through the Advanced Research Projects Agency–AT&T Cooperative Hybrid-SEED Program (ARPA–AT&T–CO-OP) workshop.[18] A schematic diagram of the unfolded optical layout of the system is shown in Fig. 1. (This figure is slightly misleading because the printed circuit boards should lie in the plane of the page and the OPS's perpendicular to the page). The polarization-based optical interconnect routes the optically encoded data from one stage to the next by means of polarization optics.

A close-up of one stage is illustrated in Fig. 2. The focused spot array generated by the OPS was first collimated by microlenses (125 μm × 125 μm) of the first pixelated mirror–lenslet array (LA1). The light comprising the spot array needed to be circularly polarized such that, after passing through the first quarter-wave plate (QWP 1) (oriented at 45° in the x–y plane), it became linearly (p) polarized. After passing through the polarizing beam splitter (PBS) and the second quarter-wave plate (QWP 2), which recircularizes the polarization, the beam array was then focused onto the hybrid-SEED SPA device residing on the printed circuit board by the second lenslet array (LA2).

The reflected (modulated) light was then recollimated through LA2 and its polarization linearized to s polarization through QWP 2. On entering the PBS, the s-polarized light then was reflected off the PBS mirror, to be routed to the next stage.

Figure 2 also illustrates the light relayed from the previous stage. This light, still s polarized, reflected off the PBS mirror surface toward LA1 after passing through QWP 1, which circularized its polarization. The beams then hit the pixelated mirrors on LA1 and passed through the same optical path as did the light from the OPS (as described above). The relayed beams, however, are displaced (in the x direction) 125 μm away from the OPS beams, thus impinging on receivers (as opposed to modulators) on the hybrid-SEED SPA.

The QWP 1, PBS, and QWP 2 were glued into what was collectively called the PBS–QWP assembly. The PBS–QWP assembly, LA1, and LA2 were mounted onto an optomechanical housing called the lenslet barrel, which, along with the OPS module, resided within a larger housing called the outer

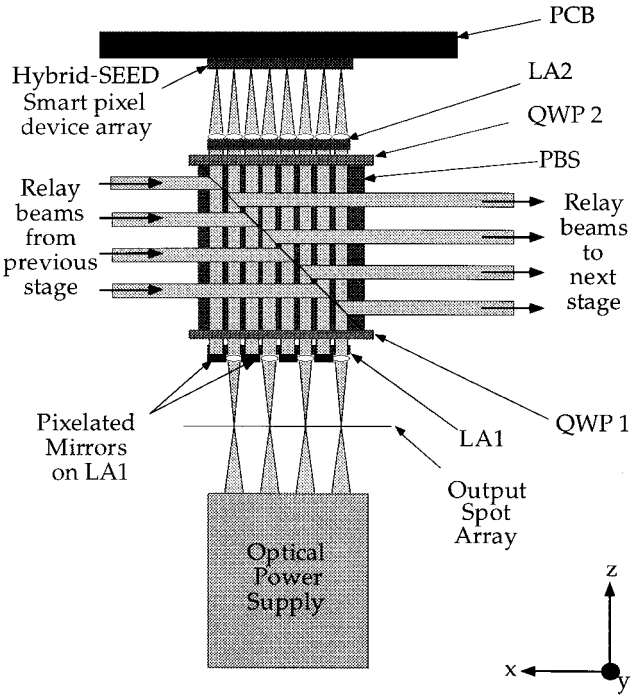

Fig. 2. Close-up of one stage of the system.

barrel. Furthermore, the system was designed to operate in a temperature-controlled environment, eliminating most concerns about effects such as thermal drift and changes in focal length.

B. Spot-Array Requirements

The layout of the 16 dual-rail smart pixels (i.e., 32 modulators) on the chip[15] was on an 8×4 grid pitched 125 μm in the vertical direction and 250 μm in the horizontal direction. The 32 modulator windows had a dimension of 20 μm × 20 μm and represent the targets for the spot array that has passed through the PBS–QWP assembly and the lenslets.

The requirements of the spot array at the output of the OPS to permit the array to hit the target modulators on the chip are given in Table 1, and a schematic diagram of the desired spot array (looking in the direction of light propagation) is shown in Fig. 3. Note that, in Fig. 3, the central grid of 8×4 represents the signal spots, while those on the periphery correspond to alignment spots. Although the requirements listed in Table 1 suffice for the designed system demonstrator, it was desired that the optical design be flexible to accommodate a larger array of target modulators for scalability.

C. Optomechanical Requirements

The system was built on a vertically mounted baseplate housed in a standard 19-in. (114-cm) 6U VME commercial backplane chassis.[19] On the basis of the high level of integration, the OPS modules needed to be compact, robust, easy to assemble, and modular.

3. Light Source

As shown in Fig. 1, the system was a four-stage optical backplane, with each stage requiring an OPS to provide the array of constant optical power beams to illuminate the modulators on the respective hybrid-SEED chips. For simplicity, optomechanical compactness, and ease of prealignment, light was launched into the OPS by means of a single-mode polarization-maintaining (PM) fiber. For practical purposes a single 500-mW tunable laser (with an external grating for wavelength selection and stabilization) was used to provide the light for all four stages. The light originally was split to the four stages by use of a tree of three 1:2 fiber splitters. However, owing to power-loss and polarization instabilities this arrangement was rejected.

A second light-splitting arrangement was employed with three (linear-polarization-preserving) pellicles (Fig. 4), which incurred no significant power losses or polarization instabilities. Each beam was subsequently coupled into a 1-m-long PM single-mode fiber to provide the optical input to each OPS module. Launching light along the PM fiber's fast axis was verified experimentally to provide better polarization stability at the output compared with launching along its slow axis. A Faraday isolator was used to eliminate backreflections into the laser. The wavelength was maintained to within the 850-nm ±1-nm spectral tolerance required for the SEED's.

Table 1. OPS Spot-Array Requirements

Characteristic	Requirement
Number of spots	• 8×4 focused spots on a uniform grid of 125 μm (vertical) × 250 μm (horizontal) • 8 additional peripheral spots to hit lenslets on LA1 (Fig. 2)
Spot-array position	Between 18.34 ± 0.82 mm away from the output of the OPS
Spot radii	6.47 μm ($1/e^2$ irradiance)
Spot-generation speed	Slower than f-6 beams generating the spot array
Light polarization	Stable, right-hand circular polarization
Field curvature	Minimal field curvature of the spot array
Power per spot	Greater than 250 μW
Power uniformity	Across the entire array, greater than 90%
Beam-steering capabilities	Lateral translation: ±400 μm Angular deviation: ±0.46°
Spectral tolerance	850 ± 1 nm

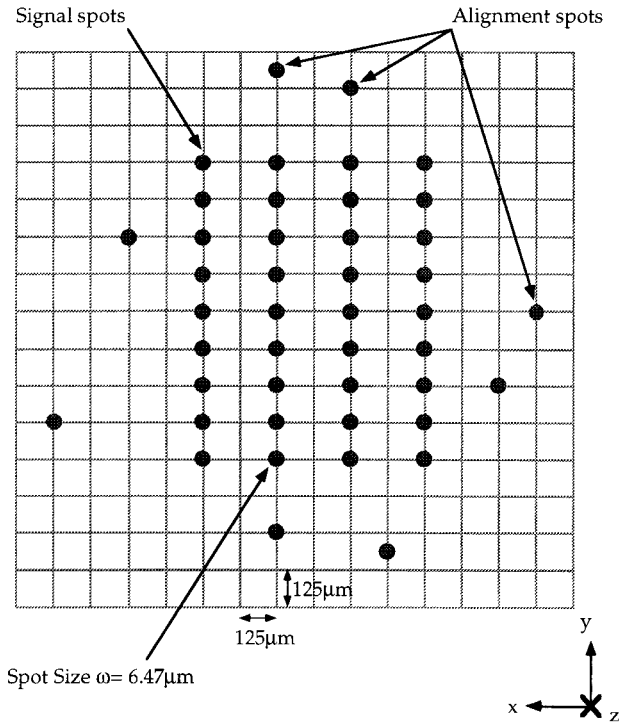

Fig. 3. Schematic of the desired spot array at the output of the OPS.

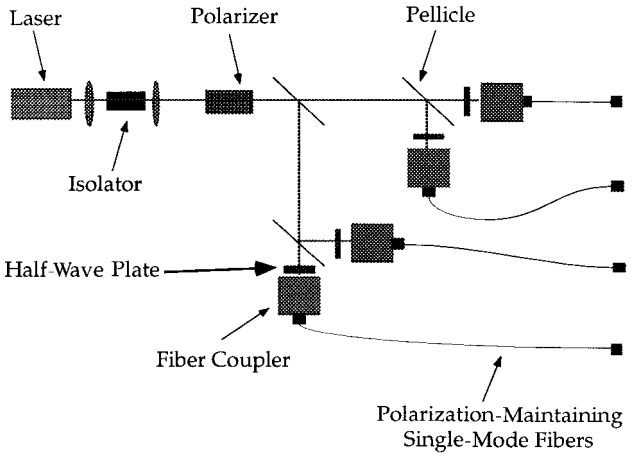

Fig. 4. Light-distribution system that uses pellicles.

4. Optical Design

The fundamental challenge of designing the OPS was in the generation of the array of 8 × 4 (plus 8 alignment) spots such that the 6.47-μm ($1/e^2$ irradiance) radii spots were positioned accurately across the 125-μm grid with a uniform power distribution. There exist numerous techniques for producing spot arrays from a single beam.[20,21] Our system employed Fourier plane array generation by use of a computer-generated hologram implemented as a multiple-level phase grating (MPG).

A. Multiple-Level Phase-Grating Design

The MPG was designed by use of a simulated-annealing algorithm[21,22] to create a grating composed of a periodic array of unit cells that could generate the desired spot array in the focal plane of a Fourier transform lens. The grating itself represented the two-dimensional spatial inverse Fourier transform of the spot array and was placed at the front focal plane of the Fourier lens.

The periodicity P of the grating is related to the spot spacing S in the Fourier plane (i.e., the output focal plane of the Fourier lens) by the relation given in Eq. 1, where λ is the wavelength and f is the focal length of the Fourier lens. The factor of 2 in the formula arises because only even-order spots were used in the grating design:

$$P = \frac{2f\lambda}{S}. \tag{1}$$

For the system demonstrator requiring a spot spacing of $S = 125$ μm (on the smallest grid, as shown in Fig. 3) for the array of 8 × 4 spots and on the basis of the chosen optical design, each unit cell had a periodicity of $P = 377.8$ μm × 377.8 μm, divided into 128 × 128 pixels. Each square pixel had a dimension of $P/128 = 2.95$ μm × 2.95 μm and a height quantized to one of eight levels. The MPG was made from fused silica and was not antireflection coated owing to time constraints.

From the design program the theoretical efficiency of the eight-level phase grating was predicted to be 83% (76.5% after the 4% reflections at each nonantireflection-coated surface). The overall uniformity of the spots was predicted to be 96.9%, as defined by use of the metric

$$\text{Uniformity} = 1 - \frac{(P_{\max} - P_{\min})}{(P_{\max} + P_{\min})}. \tag{2}$$

Defining the collimated-beam diameter passing through the MPG to be ω_{MPG} leads to the number of MPG periods sampled NPS being defined as

$$\text{NPS} = \frac{2\omega_{\text{MPG}}}{P}. \tag{3}$$

Also, from Gaussian beam-propagation models, the focused-spot radius ω_f is related to the collimated-beam diameter by

$$\omega_f = \frac{f\lambda}{\pi\omega_{\text{MPG}}}, \tag{4}$$

where f is the focal distance of the Fourier lens and λ is the wavelength.

The (linear) compression ratio CR can be defined as the ratio of the spot separation to the 99% spot diameter:

$$\text{CR} = \frac{S}{3\omega_f}. \tag{5}$$

Thus substituting Eqs. (1), (3), and (4) into Eq. (5) yields a relation between the compression ratio CR and the number of periods sampled NPS derived as

$$\mathrm{CR} = \frac{\pi}{3}\,\mathrm{NPS}. \tag{6}$$

The number of periods sampled was NPS = 6.1, where ω_{MPG} was designed to be 1.15 mm, yielding a compression ratio of 6.37 through the relation given in Eq. (6).[23] This value is sufficiently larger than the minimum $\mathrm{CR}_{\mathrm{min}}$ of 3, which is required to ensure that the power uniformity is not degraded by aliasing.[24]

We addressed the issue of scalability by ensuring that a spot array of 16 × 8 spots at one half the spot spacing (i.e., S = 62.5 μm) was implemented by replacement of the MPG element alone, with no other modifications to the optical design. On the basis of this requirement the period P of the MPG would be doubled, thereby reducing the NPS to 3.05. This results in a compression ration of CR = 3.19, which is still larger than the $\mathrm{CR}_{\mathrm{min}}$ of 3.

B. Optical Design

The optics were designed to meet all the spot-array requirements while reducing the optomechanical complexities to a minimum. They are shown schematically in Fig. 5. Perfectly linearly polarized light was assumed to be emitted from the single-mode PM fiber placed at the front focal plane of the compound collimating lenses (CL 1 and CL 2). The mode-field diameter ($1/e^2$ diameter) of the fiber was specified to be 5.6 μm. The collimated-beam diameter at the output of the collimating lens was designed to be 2.30 mm. After passing through the zero-order QWP to circularize its polarization, the beam was then passed through the MPG. The angularly diffracted collimated beams then propagated through the Risley beam steerers (RBS 1 and RBS 2) and tilt plates (TP 1 and TP 2) until they were focused by the compound Fourier lenses (FL 1 and FL 2) to spots in the Fourier plane of 6.47 μm ($1/e^2$ radii).

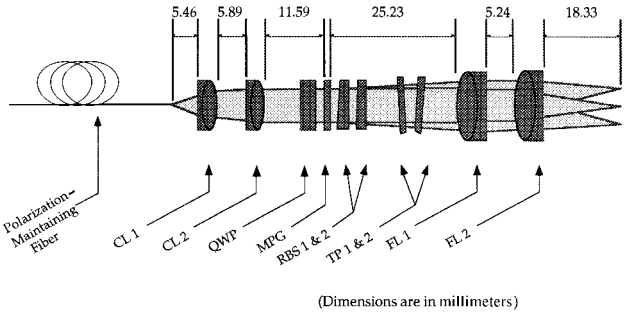

Fig. 5. Optical design of the OPS.

Two-element compound lenses with variable focal lengths were chosen for both the Fourier lenses and the collimating lenses to account for uncertainties in the mode-field diameter of the input fiber, the lens focal-length specifications, and aberrations of the beams passing through the OPS. The lenses were oriented in the Petzval configuration,[25] which provided the best performance in terms of aberrations, flexibility, optical power division, size, and cost.

In the Petzval configuration the optical power is split equally between the two parts of each compound lens. Hence aberration is minimized, and the focal length of a lens is easy to adjust with high resolution by alteration of the air gap. Although a Plossl configuration is similar, simulations showed that, in our application, the Petzval configuration gave fewer aberrations for each spot. A Cooke's triplet, which was used in an earlier modulator-array application,[26,27] was another option for the Fourier lenses because of its exceptionally flat field. However, commercial Cooke's triplets have their focal lengths specified to only ±1%, compared with the 0.4% required for the OPS optical design to define the correct spot separation. Since the optical power in a Cooke's triplet is divided unequally across the three elements, adjust-

Table 2. Optical and Optomechanical Degrees of Freedom

Detailed Design Requirement	Optical–Optomechanical Solution
Spots on a uniform grid	Choose a low-distortion Fourier lens
Spot separation matched to SEED separation	Adjust the focal length of the Fourier lens by a change in the element separation
Collimated beam through the planar elements	Maintain the fiber facet at the front focus of the collimating lens
Wave-front flatness of less than λ/20	• Choose a low-aberration Fourier lens • Keep aberrations from other elements low • Maintain the fiber at the front focus of the collimating lens
Angular alignment of the spot array about the optical axis	Rotate the MPG about the optical axis
Pitch and yaw alignment of the spot array with respect to the interconnect	Adjust the difference in the roll position of the opposed tilt plates
Mutual angular alignment of the chief rays	• Position the MPG at the front focus of the Fourier lens • Choose a low-distortion Fourier lens
Lateral alignment of the spot array	Rotate the Risley prisms about the optical axis

Table 3. Simulation Results and Tolerance Values

Simulation	Tolerance for 1% Clipping	On-Axis Spot	Corner Spot of On-Axis Array	Spot 1152-μm Off-Axis
Distortion	±2.5 μm	0 μm	0 μm	1.03 μm
Field curvature	±63 μm	0 μm	11.5 μm	46 μm
Spot size	±0.25 μm	6.47 μm	6.50 μm	6.75 μm
Chief-ray angle	±0.7°	0°	0.0008°	0.0068°
Strehl ratio	0.8	0.865	0.857	0.817
1/rms OPD	14	43.2	43.5	28.9

ing the focal length requires extremely fine changes to the element spacings.

At their nominal (Petzval configuration) positions, the compound collimating lens had a focal length of 12.90 mm and the compound Fourier lens had a focal length of 27.78 mm. It should be noted that, although a true Fourier lens should introduce an $f \sin \theta$ distortion, at the maximum diffracted angle designed to be 0.0068° within the OPS the small-angle approximations hold. Therefore an off-the-shelf lens pair was used because of cost and convenience.

On the basis of the nominal numbers used in the optical design, the *f*-number of the focused beams at the output of the OPS was $f = 12.07$ ($1/e^2$ diameter of 2.30 mm). This value is well within the *f*-6 window demanded by the lenslets. The OPS optical and optomechanical design had a number of optical and mechanical degrees of freedom to meet the set of design requirements; these are presented in Table 2. The overall theoretical throughput of the OPS was estimated to be 71.4%. By analysis of these optical and optomechanical degrees of freedom, as well as of the OPS-module requirements listed in Section 2, a barrel design was chosen to house the elements of the OPS. More information about the optomechanical design is presented in Section 5.

C. Design Tolerancing and Simulation

The total estimated lateral error of the position of the spot array with respect to LA1 (Fig. 2) was ±400 μm. This value was calculated from the worst-case estimate of the fiber centering within the OPS barrel of ±100 μm, which results in a ±230-μm error of the spot array at the output of the OPS. As well, because of the precision to which the OPS barrel could be inserted in the outer barrel with respect to LA1, machining tolerances, and centering of the lenses, an additional ±170-μm lateral-positioning error results. This corresponds to a 0.54° minimum required wedge angle for the Risley prisms (SF10 glass). Wedge angles of 1° were chosen owing to availability and cost.

Angular misalignment of the fiber input was estimated to be 1° in the worst case, yielding a 0.46° angular deviation from the optical axis of the chief rays of the output spots. For compensating this misalignment, a 3-mm-thick tilt plate (SF10 glass) oriented at 10.4° with respect to the optical axis was required. Traditional tilt-plate design requires one parallel planar optical element to have rotational degrees of freedom along the two axes perpendicular to the optical axis (pitch and yaw). This approach was not well suited to the barrel housing chosen for the

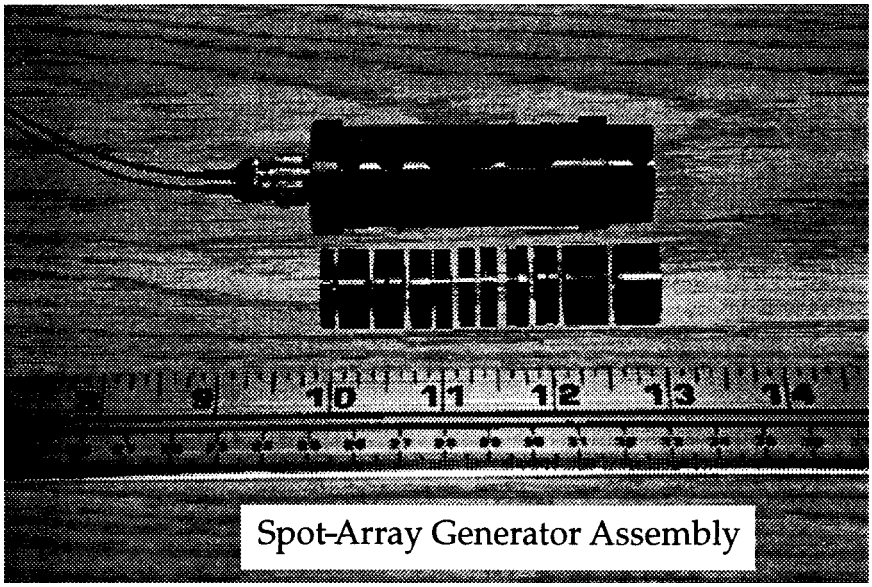

Fig. 6. Photograph of the unassembled OPS.

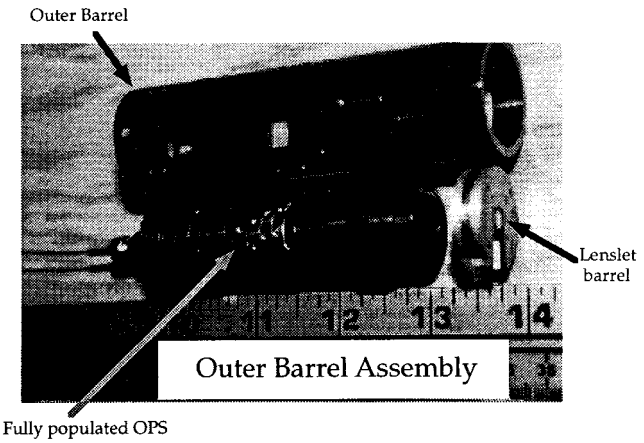

Fig. 7. Photograph of the fully populated OPS, outer barrel, and lenslet barrel.

OPS, which only conveniently provides optomechanical degrees of freedom in translation along the optical axis and rotation about the optical axis (roll). Therefore, a novel two-element tilt-plate design was implemented that requires only one degree of freedom, namely roll. These two elements are shown as TP 1 and TP 2 in Fig. 5. We achieved angular coverage of the spot array across the Fourier plane by permanently mounting two 1.5-mm-thick tilt plates (SF10 glass) at a fixed angle of 10° (from the optical axis) and by appropriately positioning both elements in roll.

Gaussian beam-power clipping of 0.54% arising from the square apertures of the system (lenslets and modulator windows) was taken into account in the optical design. A full analysis of beam propagation through the optical interconnect showed that a 1% clipping effect is tolerable as long as the spot size is kept within tight tolerances.

The system was modeled by use of a computer ray-tracing package (OSLO PRO from Sinclair Optics). Distortion of the spot array from the correct grid, field curvature, spot-size variation, Strehl ratio, 1/rms optical path difference (OPD), and variation of the chief-ray angles was calculated. The spot size was estimated with OSLO PRO as the point-spread function at the plane of best focus (minimum rms OPD). In the point-spread-function calculation a Gaussian apodization was applied at the first surface of the collimating lens. The width of this Gaussian function was given by a paraxial Gaussian calculation starting from a waist at the fiber facet.

On the basis of the lateral adjustment provided by the Risley prisms, the simulation was carried out with account taken of a maximum lateral displacement of the spot array of 575 μm. Table 3 lists a summary of results of the simulation with the nominal design parameters shown in Fig. 5. For each simulation the calculated number for a spot located directly on the optical axis, a corner signal spot of an on-axis spot array, and a spot located 1152 μm away from the optical axis (representing the outer corner spot of a 575-μm diagonally shifted spot array) is given, along with the allowable tolerance values based on 1% clipping of the beams by the modulator windows (on the hybrid-SEED chip, as shown in Fig.

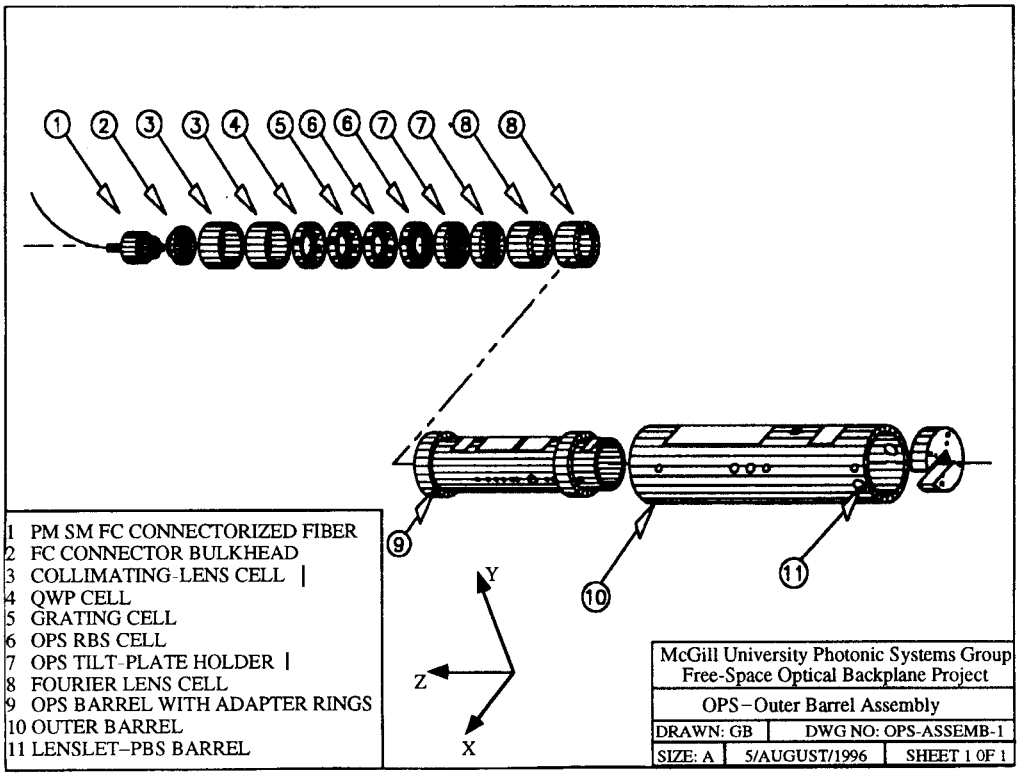

Fig. 8. Three-dimensional mechanical drawing of the OPS, outer barrel, and lenslet barrel.

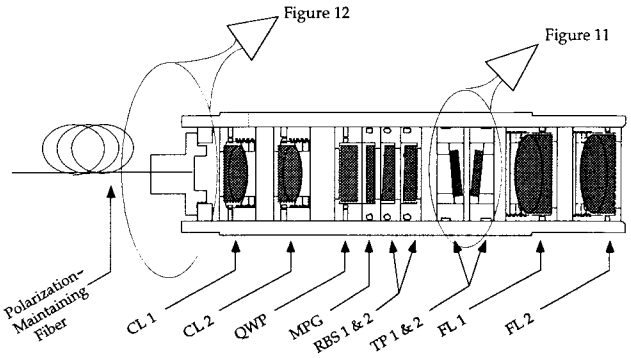

Fig. 9. Cross section of the OPS.

2). Note that the tolerances for the minimum Strehl ratio and wave-front 1/rms variation (1/rms OPD) were set at 0.8 and 14, respectively (from Ref. 1, p. 271, and Ref. 28).

It is shown in Table 3 that all simulation results (but one) for distortion, field curvature, spot size, chief-ray angle, Strehl ratio, and wave-front 1/rms variation fall within the tolerance limits for clipping of 1%. (Note that both the wave-front 1/rms variation and Strehl-ratio tolerances represent the minimum acceptable value.) The spot size for the 1152-μm diagonally shifted spot shows a simulation result of 6.75 μm, which is 0.03 μm larger than the maximum tolerance. As is shown in Sections 5 and 7, it was not necessary to displace the spot array this far. Note that the ±2.5-μm distortion tolerance represents the maximum diagonal distortion for the corner spots, which corresponds to a tolerance for spot separation of 125.00 ± 0.54 μm.

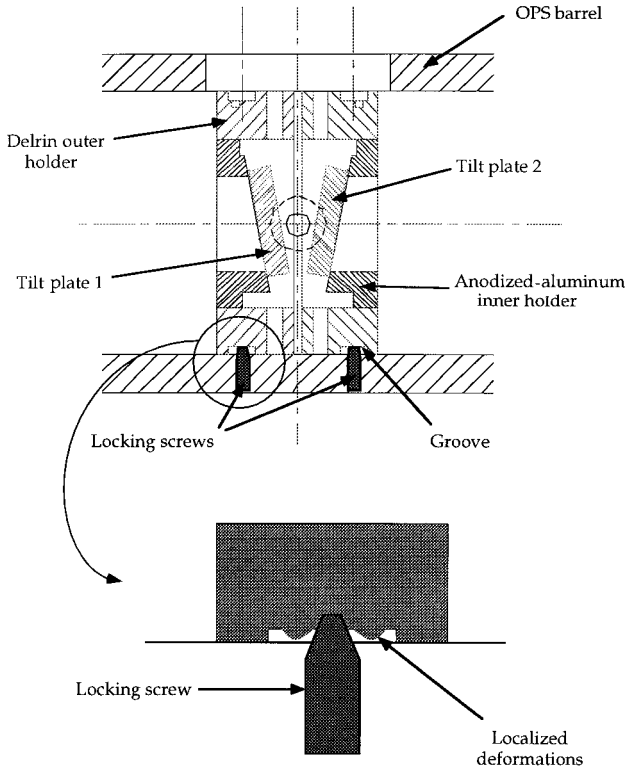

Fig. 10. Tilt-plate cell design.

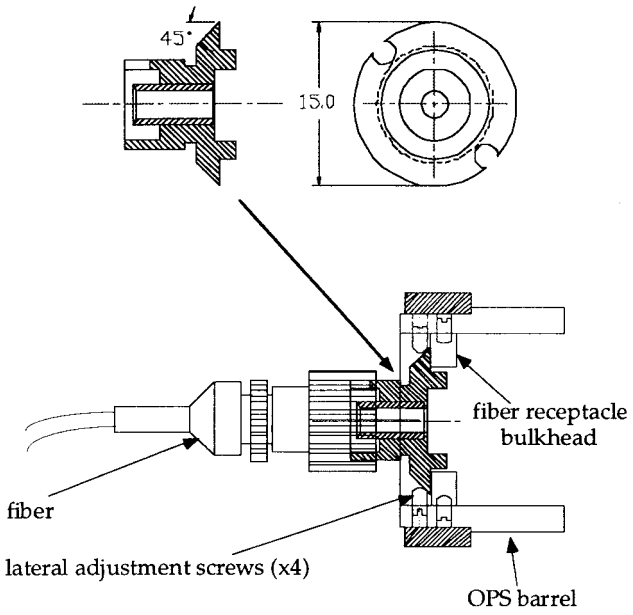

Fig. 11. Fiber-centering mechanism.

5. Optomechanical Design

A. Optical Power Supply Barrel

Given the optical design described in Section 4, the optomechanical design of the overall system demonstrator, and the overall specifications outlined in Section 2, a barrel assembly was employed to house the OPS components. A picture of the dismantled OPS is shown in Fig. 6, and the fully assembled OPS, along with the outer barrel and the lenslet barrel, is shown in Fig. 7. One of the advantages of the barrel was that all the optical components except for the last surface of the second Fourier lens were fully protected. A three-dimensional mechanical drawing of the OPS components, the OPS barrel, the outer barrel, and the lenslet barrel is given in Fig. 8, and a cross-sectional drawing of the assembled OPS is provided in Fig. 9.

For ease of machining the barrels were made out of aluminum and subsequently black anodized. The black anodization served to increase the hardness of the aluminum surface and to reduce any unwarranted glare. Two Delrin (acetal)[29] rings were then press fitted onto each barrel to facilitate the barrels' insertion into their respective outer barrels. Windows with a width of 12.6 mm were machined at the tops of the barrels to permit access to the optics' cell holders for alignment (most clearly shown in Fig. 8). Standard threaded holes (0-80 and 2-56) were machined along the two sides of the barrel such that steel set screws could securely hold each optic aligned in place. The thickness of the OPS barrel wall was 2.5 mm ± 0.1 mm; the inner diameter was 17 mm.

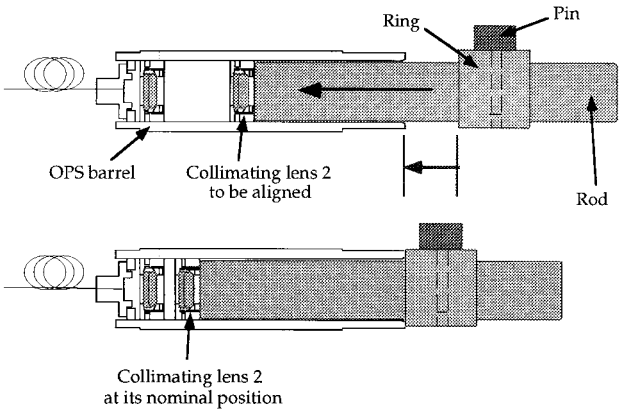

Fig. 12. OPS insertion slug.

B. Cell Holders

The cell holders were machined to provide a sliding fit to the barrel. For providing access for alignment (in rotation about and translation along the optical axis), eight holes along each cell's perimeter were machined. All the cells except those for the lenses and the tilt plates were fabricated entirely by use of anodized aluminum. The cells for the lenses were machined from Delrin such that an interference fit between the cell and lens-edge surfaces securely held each lens in place. Experimental validation of the position of the 50-mm Fourier lens within its cell showed that a 50-μm circle was described by the focused spot when the cell was rotated about the axis of an input collimated He–Ne laser beam.

One of the problems encountered with the cell-holder design was that localized deformations about the screw–cell contact point occurred on the cell surface. The raised material about the contact point had the effect of reducing the sliding-fit clearance necessary, resulting in jamming. More sophisticated cells for the tilt plates that took this into consideration are shown in Fig. 10. The tilt-plate cell incorporated a hybrid design of both Delrin and anodized aluminum: Delrin was used for the outer holder, and anodized aluminum for the inner holder. The anodized-aluminum inner holder was machined at 10° to the optic–metal interface. A groove along the perimeter of the outer holder provided the clearance necessary such that localized deformations about the screw–cell contact point did not cause the cell to get stuck within the barrel. The outer holder was machined to provide a tight interference fit with the inner holder.

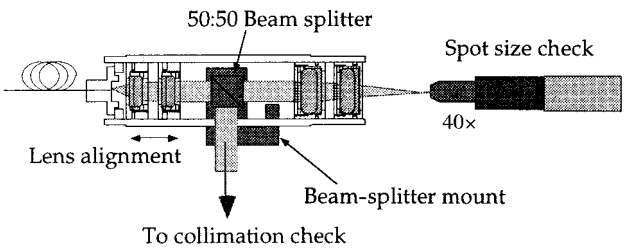

Fig. 13. Alignment of the collimating lenses.

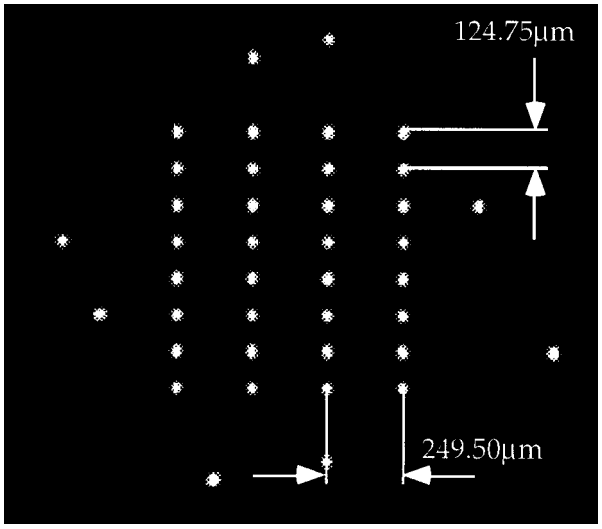

Fig. 14. Frame-grabbing of the generated spot array.

C. Fiber Mount

A close-up of the mechanism for centering the fiber on the optomechanical axis of the barrel is shown in Fig. 11. A high-quality fiber-connector–physical-contact (FC/PC) fiber receptacle was chamfered down at 45° into a circle with a 15-mm diameter. Butted up against the fiber-receptacle bulkhead (made of anodized aluminum), which was locked into place in the barrel, were four set screws driven against the chamfered edge for making lateral adjustments. Centering to better than 10 μm from the optomechanical axis was achieved and is well within the ±100-μm design tolerance. Stability measurements were conducted on insertion and removal of the connectorized input fiber, and no measurable misalignment within the ±1-μm measurement precision was observed.

6. Assembly and Alignment

The first stage of the alignment procedure was to launch the linearly polarized light into each PM fiber along its fast axis. This was achieved by rotation of the half-wave plate (as shown in Fig. 4).

Assembly of the OPS was simplified by use of the OPS insertion slug. The insertion slug was composed of three pieces: the rod, the ring, and the pin. Positioning the ring at the appropriate position on the rod by means of pushing the pin through accurately machined holes in the rod allowed each element to be inserted into the barrel from the output side of the barrel, as shown in Fig. 12. When the ring butted up against the output end of the barrel, it was in place. Component-placement precision was better than ±90 μm.

A two-step alignment sequence was required to assemble the components of the OPS within the barrel. For properly collimating the beam and providing the correct spot size at the output of the OPS, adjustment of the two collimating lenses was required. For monitoring both these effects simultaneously, the OPS barrel with the precentered fiber

Table 4. Spot and Spot-Array Characterization[a]

OPS Barrel	Average On-Axis Center Spot: ω (6.47 ± 0.25 μm)	Average On-Axis Center Spot: Percent G (NA)	Average On-Axis Center Spot: z (NA)	Average On-Axis Corner Spot: ω (6.47 ± 0.25 μm)	Average On-Axis Corner Spot: Percent G (NA)	Average On-Axis Corner Spot: z (<63 μm)	Corner Spot: 685-μm-Shifted Spot Array: ω (6.47 ± 0.25 μm)	Corner Spot: 685-μm-Shifted Spot Array: Percent G (NA)	Back Focal Length (18.34 ± 0.82 μm)	Separation (125 ± 0.6 μm)	Power Uniformity (>90%)
1	6.47	93.9	0	6.68	90.6	19.3	7.04	94.1	18.1	124.8	NA
2	6.61	96.1	0	6.62	96.3	11.5	6.68	95.4	18.0	125.2	NA
3	6.49	98.1	0	6.47	96.1	38.8	6.80	93.7	18.0	125.2	92.8
4	6.52	94.2	0	6.57	96.0	0.3	6.53	97.0	18.3	124.9	92.9

[a]NA, not applicable. The values in parentheses represent the tolerances of those parameters.

was populated with only the four lenses, positioned at their nominal positions by use of the insertion slug. The Fourier lenses were locked in place. The remaining six elements were not inserted, and in their place a 10-mm 50:50 beam splitter was inserted through the windows, as shown in Fig. 13.

Spot sizes were measured with a 40× microscope objective imaging onto a high-resolution linear CCD camera accurately positioned by motorized *x–y–z* stages. The CCD image was digitized for the measurements.

After the collimating lenses were locked, the beam splitter and the Fourier lenses were removed. Each barrel was then fully populated with the QWP, MPG, Risley prisms, tilt plates, and Fourier lenses, with the prisms and tilt plates at their zero positions. Alignment of the QWP was done *in situ* after the OPS was integrated into the system to maximize transmission through the PBS–QWP assembly. It should be noted that locking the collimating lenses modified the spot size by ±0.10 μm on average. Spot separation was set by adjustment of the second Fourier lens, measured by use of the same CCD setup with the 40× microscope objective.

7. Characterization

Detailed performance measurements were conducted on the four assembled barrels to obtain statistical information on the reproducibility of the design and implementation. The results are presented below. A digitized image (from the frame grabber) of the spot array generated from barrel 1 is shown in Fig. 14. Note that the image appears to be flipped in the horizontal direction in comparison with Fig. 3 because of the direction of observation and the inversion introduced by the imaging optics.

A. Spots and Spot Array

As mentioned in Section 6, the frame-grabbed spots were curve fitted to a Gaussian beam model. This algorithm provided the $1/e^2$ irradiance spot size. It also calculated the Gaussian fit, which was obtained by performance of a chi-squared metric between the measured (quantized) data and the best-fit Gaussian curve.[30,31]

The results of characterization for the four assembled and prealigned OPS barrels are summarized in Table 4. For each barrel the information is presented as follows: Average spot size (±0.10 μm), average Gaussian fit, and average axial position (±15 μm) of (a) the four central spots of an on-axis spot array, and (b) the four corner spots of an on-axis spot array. Note that the average axial position of the corner spots is a direct measure of the field curvature introduced to the on-axis spot array (with the origin set as the average for the four central spots). The measured spot size and Gaussian fit for a corner spot of a 685 μm diagonally shifted spot array is also presented (with 685 μm representing the maximum possible lateral shift achievable with the Risley prisms, as is mentioned below in this section). The back focal length (i.e., the distance between the last lens surface to the spot array) is given (±0.1 mm) for each barrel. The last two columns in Table 4 are the

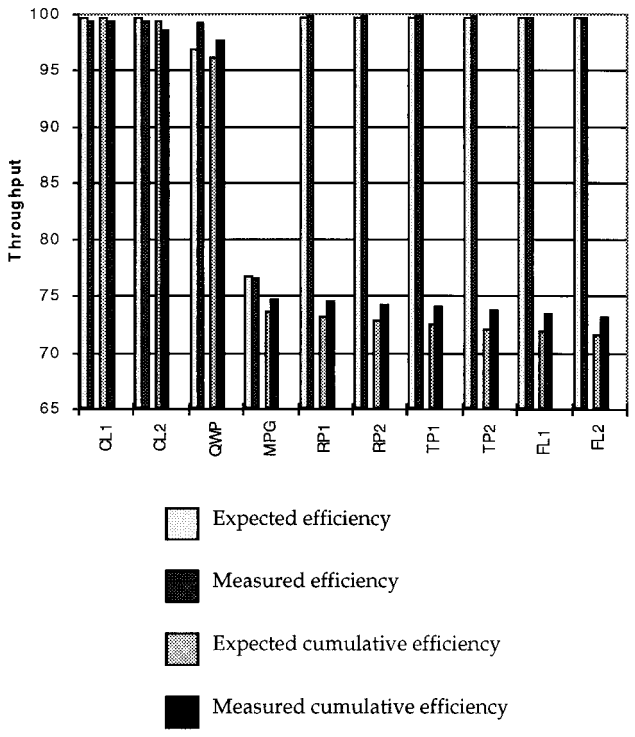

Fig. 15. Graph of the optical power budget.

Table 5. OPS Spot-Array Requirements and Characterization Results

Requirement	Characterization for the Four Barrels
8×4 focused spots on a uniform grid of 125.00 μm × 250.00 μm (±0.54 μm)	8×4 spots on a uniform grid: Minimum of 124.8 μm and maximum of 125.2 μm in the vertical direction
Eight additional alignment spots	Achieved by means of the MPG design
Back focal length of 18.34 ± 0.82 mm	Minimum of 18.00 mm and maximum of 18.30 mm
Spot radii ($1/e^2$ irradiance) of 6.47 ± 0.25 μm	• Minimum center spot size: 6.5 μm • Maximum center spot size: 6.6 μm • Minimum corner spot size: 6.5 μm • Maximum corner spot size: 6.7 μm
Beams slower than *f*-6 beams to generate the spot array	*f*-12 spots generated
Stable right-hand circularly polarized light	Achieved *in situ*
Minimal field curvature of <63 μm across the spot array	• Minimum field curvature: 0.3 μm • Maximum field curvature: 38.8 μm
Power per spot of greater than 250 μW	900 μW/spot (See Section 8)
Power uniformity across the entire array of greater than 90%	Array power uniformity >92%
Beam-steering capabilities of greater than (a) ±400-μm lateral translation (b) ±0.46° angular deviation	Beam-steering capabilities of (a) ±685-μm lateral translation (b) ±0.49° angular deviation
Spectral tolerance of 850 ± 1 nm	Within the stated requirement

spot separation (±0.2 μm) and power uniformity (±1.0%), respectively. For convenience, the tolerances for the spot size, field curvature, back focal length, spot separation, and power uniformity are included in the headings of the appropriate columns.

The power uniformity of the spot arrays was obtained from a frame-grabbed image by use of the linear high-resolution CCD camera. The image was fed into a program that computed the integrated power per spot by summing the pixel elements within each spot's elementary cell (of 125 μm × 250 μm). Thus the total integrated power of each spot was measured and compared. This integration was necessary since it was found to be difficult to match the plane of the spot array to the plane of the CCD active area directly, resulting in a spatially defocused image. Power-uniformity measurements for barrels 1 and 2 were unavailable as they had already been integrated into the system. Noting the negligible statistical difference (to within measurement precision) between the measurements for barrels 3 and 4, however, it was expected that the MPG's for barrels 1 and 2 would behave similarly, and the power uniformity was better than 92.0% at the OPS output.

Table 4 indicates that all measurements but two fit within the specified tolerances. The spot size of an outer corner spot of a 685 μm diagonally shifted spot array was measured to be 7.04 μm for barrel 1, and 6.80 μm for barrel 3, both larger than the allowable tolerance. If we note, however, that, since the fiber was centered to better than 10 μm within the OPS barrel (as presented in Section 5), compared with the ±100 μm tolerance (as presented in Section 4), it would be necessary only to shift the spot array laterally by at most ±200 μm.

B. Spectral Behavior

Preliminary tests have shown that there was no significant effect caused by the backreflections from the OPS components on the spectral behavior of the laser. The Faraday isolator (Fig. 4) provided a nominal −40 db of isolation and was required to achieve this lack of effect.

C. Polarization

During assembly when only the two collimating lenses and the QWP were present in the OPS barrel, the orientation of the QWP was adjusted to bring the emerging light as close as possible to ideal circular polarization. Measurements conducted on a PBS–QWP assembly at the output indicated a light throughput of 95%, with the missing 5% attributed to factors such as the transmission efficiency of the PBS (96% for *p* polarization), the finite extinction ratio of the PM fiber (28.8 dB), and improper orientation of the QWP's (both of the ones attached to the PBS by the supplier and of the one in the OPS itself). Polarization stability is demonstrated by the small (<0.5%) time variation of the transmitted light.

D. Beam Steering

Measurements conducted on the lateral steering travel of the Risley prisms on the spot array yielded results of ±685 ± 3 μm from the optical axis. Measurement results for the angular-steering coverage of the tilt plates were ±0.49° ± 0.08°. These values are better than the ±400 μm and 0.46° lateral- and angular-steering requirements, respectively, as specified in Table 1, to compensate for the alignment errors encountered during the integration of the OPS into the system.

E. Optical Power Budget

Each optical element in barrel 3 had a measured optical throughput efficiency of better than 99%, except for the fan-out grating, which had an efficiency of 76.5%. These results are plotted in Fig. 15. The overall throughput was measured for barrel 3 and found to be 73.0% ± 0.5%, consistent with expected values.

8. Discussion and Conclusion

It has been shown that an easy-to-assemble, scalable, robust, compact, and modular OPS spot-array generator was successfully built to drive an array of 32 hybrid-SEED modulators for use in a four-stage optical interconnect. The success is based on meeting the specifications that are presented in Table 1. This table is presented again in Table 5, along with the characterization results. We satisfied the power requirement (the seventh item in the list) by taking into account the measured optical losses experienced by the laser beam's passing through the optical train (Fig. 4) of 78.6% and loss at the fiber coupler, which was at its worst 50%. Based on the laser source's providing 500 mW, this results in spots at the output of the OPS of 900 μW, more than 3 times the required power. It should be noted that the optical interconnect, i.e., light originating from the OPS through to the hybrid-SEED chip on the first stage, through the optics to the hybrid-SEED chip on the second stage, was established, demonstrating that the requirements for the OPS were satisfied.

Future optical interconnects most probably will employ the use of source-based transmitters (e.g., vertical-cavity surface-emitting lasers) rather than modulators. However, until then, simple and robust optical and optomechanical solutions are needed for modulator-based technology. This paper has shown that, for the first time to our knowledge, a compact modularized spot-array generator can be built for use in a modulator-based optical interconnect, successfully taking the first step in bridging the generation gap between sophisticated hybrid-SEED optoelectronics and optics.

D. V. Plant was supported by the Canadian Institute for Telecommunications Research under the National Centre for Excellence program of the Government of Canada, by the Natural Sciences and Engineering Research Council (NSERC) (OGP0155159), and the Fonds pour la Formation de Chercheure et l'Aide à la Recherche (NC-1415). This study was also supported by the Nortel/NSERC Chair in Photonic Systems. Acknowledgment is given to the ARPA–CO-OP–Honeywell DOE Workshop for the manufacture of the multiple-phase grating. D. J. Goodwill was supported by the Hudson Moore Jr. Chair at the University of Colorado. Appreciation is given to the following for their assistance: George Smith (Heriot-Watt University), who machined a subset of the optomechanics for the OPS; Heinz Nentwich (NORTEL), who sawed the multiple-phase gratings to chip-level accuracy; and special thanks to Don Pavlasek and Joe Boka (McGill University), who not only machined the majority of the optomechanics for the OPS but provided invaluable assistance in their design. R. Iyer gratefully acknowledges funding from NSERC through a Postgraduate Scholarship.

References and Note

1. H. S. Hinton, *An Introduction to Photonic Switching Fabrics* (Plennum Press, New York, 1993).
2. R. A. Nordin, F. J. Levi, R. N. Nottenburg, J. O'Gorman, T. Tanbun-Ek, and R. A. Logan, "A systems perspective on digital interconnections technology," J. Lightwave Technol. **10,** 811–827 (1992).
3. D. V. Plant, B. Robertson, H. S. Hinton, W. M. Robertson, G. C. Boisset, N. H. Kim, Y. S. Liu, M. R. Otazo, D. R. Rolston, and A. Z. Shang, "An optical backplane demonstrator system based on FET-SEED smart pixel arrays and diffractive lenslet arrays," IEEE Photon. Technol. Lett. **7,** 1057–1059 (1995).
4. T. Sakano, T. Matsumoto, and K. Noguchi, "Three-dimensional board-to-board free-space optical interconnects and their application to the prototype multiprocessor system—COSINE-III," Appl. Opt. **34,** 1815–1822 (1995).
5. D. Z. Tsang and T. J. Goblick, "Free-space optical interconnection technology in parallel processing systems," Opt. Eng. **33,** 1524–1531 (1994).
6. D. V. Plant, B. Robertson, H. S. Hinton, M. H. Ayliffe, G. C. Boisset, W. Hsiao, D. Kabal, N. H. Kim, Y. S. Liu, M. R. Otazo, D. Pavlasek, A. Z. Shang, J. Simmons, and W. M. Robertson, "A 4 × 4 VCSEL/MSM optical backplane demonstrator system," in *Proceedings of the IEEE-LEOS Annual Meeting 1995* (Institute of Electrical and Electronics Engineers, Lasers and Electro-Optics Society, La Plata, Calif., 1995), Postdeadline paper PD2.4.
7. D. V. Plant, B. Robertson, H. S. Hinton, M. H. Ayliffe, G. C. Boisset, D. J. Goodwill, D. N. Kabal, R. Iyer, Y. S. Liu, D. R. Rolston, W. M. Robertson, and M. R. Taghizadeh, "A multistage CMOS-SEED optical backplane demonstrator system," Opt. Comput. **96,** 14–15 (1996).
8. F. B. McCormick, F. A. P. Tooley, T. J. Cloonan, J. L. Brubaker, A. L. Lentine, R. L. Morrison, S. J. Hinterlong, M. J. Herron, S. L. Walker, and J. M. Sasian, "Experimental investigation of a free-space optical switching network by using symmetric self-electro-optic-effect devices," Appl. Opt. **31,** 5431–5446 (1992).
9. F. B. McCormick, T. J. Cloonan, A. L. Lentine, J. M. Sasian, R. L. Morrison, M. G. Beckman, S. L. Walker, M. J. Wojcik, S. J. Hinterlong, R. J. Crisci, R. A. Novotny, and H. S. Hinton, "Five-stage free-space optical switching network with field-effect transistor self-electro-optic-effect-device smart-pixel arrays," Appl. Opt. **33,** 1601–1618 (1994).
10. F. B. McCormick, A. L. Lentine, R. L. Morrison, J. M. Sasian, T. J. Cloonan, R. A. Novotny, M. G. Beckman, M. J. Wojcik, S. J. Hinterlong, and D. B. Buchholz, "155 Mb/s operation of a FET-SEED free-space switching network," IEEE Photon. Technol. Lett. **6,** 1479–1481 (1994).
11. F. B. McCormick, A. L. Lentine, R. L. Morrison, J. M. Sasian, T. J. Cloonan, R. A. Novotny, M. G. Beckman, M. J. Wojcik, S. J. Hinterlong, and D. B. Buchholz, "Free-space optical switching using FET-SEED smart-pixel arrays," Inst. Phys. Conf. Ser. **139,** Part II, 131–136 (1994).
12. D. V. Plant, B. Robertson, H. S. Hinton, W. M. Robertson, G. C. Boisset, N. H. Kim, Y. S. Liu, M. R. Otazo, D. R. Rolston, A. Z. Shang, and L. Sun, "A FET-SEED smart pixel based optical backplane demonstrator," Inst. Phys. Conf. Ser. **139,** Part II, 145–148 (1994).
13. S. Araki, M. Kajita, K. Kasahara, K. Kubota, K. Kurihara, I. Redmond, E. Schenfeld, and T. Suzaki, "Experimental free-

space optical network for massively parallel computers," Appl. Opt. **35,** 1269–1281 (1996).
14. K. W. Goosen, J. A. Walker, L. A. D'Asaro, S. P. Hui, B. Tseng, R. Leibenguth, D. Kossives, D. D. Bacon, D. Dahringer, L. M. F. Chirovsky, A. L. Lentine, and D. A. B. Miller, "GaAs MQW modulators integrated with silicon CMOS," IEEE Photon. Technol. Lett. **7,** 360–362 (1995).
15. D. R. Rolston, D. V. Plant, T. H. Szymanski, H. S. Hinton, W. S. Hsiao, M. H. Ayliffe, D. Kabal, M. B. Venditti, P. Desai, A. V. Krishnamoorthy, K. W. Goosen, J. A. Walker, B. Tseng, S. P. Hui, J. C. Cunningham, and W. Y. Jan, "A hybrid-SEED smart pixel array for a four-stage intelligent optical backplane demonstrator," IEEE J. Select. Topics Quantum Electron. **2,** 97–105 (1996).
16. B. Robertson, Y. S. Liu, G. C. Boisset, D. J. Goodwill, M. H. Ayliffe, W. H. Hsiao, R. Iyer, D. Kabal, D. Pavlasek, M. R. Taghizadeh, H. S. Hinton, and D. V. Plant, "Optical design and characterization of a compact free-space photonic backplane demonstrator," paper presented at the *1996 OSA Annual Meeting*, Rochester, N.Y., 20–25 October 1996, paper MLL5.
17. G. C. Boisset, M. H. Ayliffe, B. Robertson, R. Iyer, Y. S. Liu, D. V. Plant, D. J. Goodwill, D. Kabal, and D. Pavlasek, "Optomechanics for a four-stage hybrid-self-electro-optic-device-based free-space optical backplane," Appl. Opt. **36,** 7341–7358 (1997).
18. ARPA–AT&T Cooperative Project, Hybrid-SEED Workshop, 18–21 July 1995, George Mason University, Fairfax, Va., 1995.
19. IEEE Standard 1014-1987 for a Versatile Backplane Bus: VMEbus, IEEE ref. [1-55937-674-0] [SH11544-NYF] (Institute of Electrical and Electronics Engineers, New York, 1987).
20. N. Streibl, "Beam shaping with optical array generators," J. Mod. Opt. **36,** 1559–1573 (1989).
21. M. P. Dames, R. P. Dowling, P. McKee, and D. Wood, "Efficient optical elements to generate intensity weighted spot arrays: design and fabrication," Appl. Opt. **30,** 2685–2691 (1991).
22. A. G. Kirk and T. J. Hall, "Design of binary computer generated holograms by simulated annealing: coding density and reconstruction error," Opt. Commun. **94,** 491–496 (1992).
23. Y. S. Liu, B. Robertson, D. V. Plant, H. S. Hinton, and W. M. Robertson, "Design and characterization of a microchannel optical interconnect for optical backplanes," Appl. Opt. **36,** 3127–3141 (1996).
24. F. B. McCormick, "Free-space interconnection techniques," in *Photonics in Switching*, J. E. Midwinter, ed. (Academic, San Diego, Calif., 1993), pp. 185–189.
25. R. E. Fischer and W. J. Smith, *Modern Lens Design—A Resource Manual* (McGraw-Hill, New York, 1992), pp. 221–238.
26. A. C. Walker, I. R. Redmond, D. J. McKnight, R. G. A. Craig, G. S. Buller, P. Meredith, and M. R. Taghizadeh, "Construction of an optical cellular logic image processor," in *Topical Meeting on Optical Computing*, A. M. Goncharenko, F. V. Karpushko, G. V. Sinitsyn, and S. P. Apanasevich, eds., Proc. SPIE **1806,** 373–377.
27. R. G. A. Craig, B. S. Wherrett, A. C. Walker, D. J. McKnight, I. R. Redmond, J. F. Snowdon, G. S. Buller, E. J. Restall, R. A. Wilson, S. Wakelin, N. McArdle, P. Meredith, J. M. Miller, M. R. Taghizadeh, G. Mackinnon, and S. D. Smith, "First programmable digital optical processor: optical cellular logic image processor," in *Optics for Computers: Architectures and Technologies*, G. J. Lebreton, ed., Proc. SPIE **1505,** 76–78.
28. J. E. Midwinter, *Photonics in Switching* (Academic, San Diego, Calif., 1993), p. 200.
29. Delrin is a trademarked name. The mention of this brand name in this paper is for information purposes only and does not constitute an endorsement of the product by the authors or their institutions.
30. S. Wolfram, *Mathematica—A System for Doing Mathematics by Computer* (Addison-Wesley, Reading, Mass., 1991), pp. 587, 672.
31. P. G. Hoel, *Elementary Statistics* (Wiley, New York, 1962), pp. 54–67.